



Fermi National Accelerator Laboratory

FERMILAB-Conf-91/26-E
[E-741/CDF]

**Study of Vector Boson Decay and Determination
of the Standard Model Parameters
at Hadronic Colliders***

Dan Amidei
Fermi National Accelerator Laboratory
P.O. Box 500
Batavia, Illinois 60510

January 11, 1991

* To be published in the proceedings of the Xth International Conference on Physics in Collision,
Duke University, Durham, North Carolina, June 21-23, 1990.



Operated by Universities Research Association Inc. under contract with the United States Department of Energy

**STUDY OF VECTOR BOSON DECAY AND
DETERMINATION OF THE STANDARD MODEL
PARAMETERS
AT HADRONIC COLLIDERS**

Dan Amidei

Fermi National Accelerator Laboratory, Batavia, IL 60510

Abstract

The power of the detectors and the datasets at hadronic colliders begins to allow measurement of the electroweak parameters with a precision that confronts the perturbative corrections to the theory. Recent measurements of M_Z , M_W , and $\sin \theta_W$ by CDF and UA2 are reviewed, with some emphasis on how experimental precision is achieved, and some discussion of the import for the specification of the Standard Model.

1. Introduction

With the advent of high energy colliders and the production of on-shell vector bosons, we have the prospect of measuring the Standard Model parameters unhindered by the ambiguities that have plagued measurements at lower energy.

The most precise collider result to date is the the value of the Z mass derived from resonance parameters in e^+e^- annihilation[1]. At hadron colliders, vector bosons are observed only in their final state, and the precision of a mass measurement is limited by the uncertainty in the absolute detector calibration. This disadvantage is somewhat counterbalanced, however, by the copious sample of W bosons produced along with the Z in hadronic collisions. This well stocked electroweak laboratory has several utilities:

1. When higher order corrections are included, the solution to the theory requires, in addition to the Z mass, one other constraint, which could be the W mass, or $\sin^2 \theta_W$, or M_{top} . Measurement of both masses allows calculation of the other two variables.
2. The electroweak mixing parameter, $\sin^2 \theta_W$, is a function of M_W/M_Z , and the experimental mass scale error cancels in the ratio.
3. $\sin^2 \theta_W$ can also be measured via the front-back asymmetry in the decay lepton angular distribution, providing, in effect, a second completely different measurement method *in the same experiment*.
4. The LEP/SLC Z mass can be used to understand the detector mass scale error in the measurement of M_Z , enhancing the ultimate precision in the measurement M_W .

I will begin this report with a experimenter's exegesis of the issues surrounding the determination of the Standard Model parameters. I then turn to the measurment of M_Z and M_W at CDF and UA2, following Refs. 2, 3, and 4. I pay close attention to calibration issues, and will attempt to demonstrate that the power of the detectors, coupled with the richness of the data, provides *in situ* laboratories for understanding even the thorniest of systematic effects. I follow this with a discussion of a very different approach, the measurement of $\sin^2 \theta_W$ from the charge asymmetry in Z decay.

In all cases, I focus on the most precise values as derived from the recent work by CDF and UA2. For an excellent review of the situation up to 1988, see the lectures of DiLella at the 1988 Cargese Summer School[5].

2. Specifying the Standard Model

The Standard Model parameters are the fermion masses, the SU(2) and U(1) coupling constants, the scalar Higgs vacuum expectation value, and the Higgs self coupling. In a traditional transformation to a physically observable basis, the Higgs parameters become the universal Fermi constant, G_F , and the Higgs mass, M_H , and the couplings become the fine structure constant, α , and the sine of the Weinberg angle, $\sin \theta_W$. The advantage of this parameterization is obviously the precision with which α and G_F are known from measurements of $g-2$ and the muon lifetime, and the accessibility of $\sin \theta_W$ via low energy neutral current experiments.

Problems arise, however, when higher order corrections are included. $\sin \theta_W$ is defined by a variety of tree level diagrams; when higher order diagrams are added, each of these different processes yields a different value of $\sin \theta_W$. To further obscure the matter, the corrections depend on the fermion masses, and thus the unknown M_{top} .

In order to compare the results of different measurements of $\sin \theta_W$, it has become customary to adopt, as a standard, the "on-shell" renormalization convention of Marciano and Sirlin[6], where

$$\sin^2 \theta_W = 1 - \frac{M_W^2}{M_Z^2} \quad (1)$$

is true to all orders, and radiative corrections are absorbed entirely into the vector boson masses, such that

$$M_W^2 = \frac{A^2}{(1 - \Delta r) \sin^2 \theta_W} \quad M_Z^2 = \frac{A^2}{(1 - \Delta r) \sin^2 \theta_W \cos^2 \theta_W} \quad (2)$$

where A encompasses the well measured quantities

$$A \equiv \left[\frac{\pi \alpha}{\sqrt{2} G_F} \right]^{\frac{1}{2}} = 37.2805 \pm 0.0003$$

and Δr encompasses the boson self-energy corrections. These corrections again depend somewhat strongly on the fermion masses, particularly the unknown M_{top} , and weakly on M_H .

The historical utility of this scheme was its use as a renormalization standard by which different low energy neutral current experiments could recalculate and compare their different measurements of $\sin \theta_W$. Viewed in a contemporary light, however, it suggests a more contemporary basis. First, it is obvious from Eq. 1 that M_Z and M_W

in combination are as good as $\sin \theta_W$. Furthermore, if Eq. 2 is considered as a system of 2 equations in 2 unknowns, it is clear that, with large samples of real vector bosons available, the sensible input parameters are the physical masses of the W and the Z, with Δr and the poorly defined $\sin \theta_W$ then available as solutions.

With the Standard Model described, then, by the parameter set

$$\alpha, G_F, M_Z, M_W$$

the hadron collider experiments find themselves in a position to complete its specification, uncomplicated by various theoretical uncertainties (the charm quark mass, higher twist, etc.) which cloud the interpretation of low energy neutral current results[7]. $\sin \theta_W$ is now a derived quantity, as well as Δr , and through it, M_{top} . The strength of the correlation between M_W , M_Z , and M_{top} is shown in Fig. 8.[8][4] For M_Z and M_H fixed, a 200 MeV variation in M_W gives about a 40 GeV variation in M_{top} . The weak dependence on M_H is displayed for $M_{top} = 80 \text{ GeV}/c^2$, with $M_H = 25$ (dotted), 100(solid), 1000(dashed).

Note, finally, for the future, that a precise measurement of the *three* parameters M_Z , M_W , and M_{top} is somewhat overconstrained, and limits M_H and the consistency of the entire model.

3. The Detectors

The CDF detector is shown in Fig. 1, and described in detail in Ref. 9. In the region $|\eta| \lesssim 1.0$, charged particle tracking is carried out in a 1.4 Tesla solenoidal magnetic field. Vertex time projection chambers measure tracks out to radii of 22 cm and locate the position of the interaction along the beamline to an accuracy of 1 mm. An 84 layer drift chamber measures tracks between radii of 0.25 m and 1.3 m, and yields beam constrained momentum measurements with resolution $\delta p_T/p_T^2 \cong 0.1\% (\text{GeV}/c)^{-1}$.

Electromagnetic (EM) and hadronic calorimeters outside of the tracking volume are arranged in a fine grained projective tower geometry covering most of the 4π solid angle. The tower size is 15° in ϕ by 0.1 in η . In the region $|\eta| < 1.1$, a layer of proportional wire/strip chambers (STP) imbedded in the EM calorimeter at the position of shower maximum measure the position and lateral profile of electromagnetic showers. The region $|\eta| < 0.63$ is instrumented with drift chambers outside of the calorimeters for muon identification (CMU).

The UA2 detector, shown in Fig. 2, and described in detail in Ref. 4, uses a non-magnetic strategy. The central and endcap calorimeters are segmented into projective towers with granularity of 15° in ϕ and 0.2 in η , and a longitudinal segmentation into electromagnetic and hadronic compartments. In the central region, a new compact tracking system employs 2 arrays of silicon counters (SI), a cylindrical drift chamber (JVD), transition radiation detectors (TRD), and a scintillating fiber tracker (SFD). For the study of vector boson decay in the electron channel, the SFD is the most important. It has 18 tracking layers followed by a 1.5 radiation length thick lead converter, then a further 6 layers which are used to localize electromagnetic showers which begin in the converter.

4. The Measurement of M_Z

4a. Event Selection

Z bosons are isolated and measured in their decays to e^+e^- , and in CDF only, in the decay to $\mu^+\mu^-$. The selection procedures for the two experiments are outlined in Table 1. In the electron channel, both experiments use triggers which recognise local energy depositions, or clusters, that are predominantly electromagnetic and above a threshold in E_T . Both experiments have a single inclusive cluster and cluster pair trigger, with lower thresholds on the pair. At CDF, coincidence is required between the EM cluster and a charged track of modest p_T as reconstructed by a hardware trigger processor. Offline electron identification at CDF/UA2 relies on:

- Matching CTC/SFD tracks with an EM shower localized in the STP-chambers/SFD-preshower detector.
- The lateral profile of the shower in the CEM-STP/SFD.
- The longitudinal shower profile the calorimeter tower.

In addition to these procedures, CDF can also measure and cut on the ratio E/P of electron energy seen in the calorimeter and track momentum seen in the tracking system tracking.

In the muon channel, CDF triggers on the match between stubs in the central muon chambers and trigger processor tracks, and has a similar strategy of singles or pairs with high or low p_T thresholds as in the electron case. The offline identification requires a

match in position and angle between the CTC track and the CMU stub, and also that the energy deposited in both the EM and hadronic calorimeter compartments behind the muon be consistent to high efficiency with a minimum ionizing particle and possible soft hadronic overlap.

The final Z sample is derived in both experiments by requiring two central lepton candidates with an invariant mass in a broad window around the Z. To augment their statistics, UA2 allows events with one well measured central electron and another non-central EM cluster such that the total momentum balances in the direction orthogonal to the electron bisector. (The ξ axis. See Fig. 3). Momentum balance along this direction is sensitive mostly to the calorimeter resolution, and is desensitized to the poor calorimeter response to any low energy hadronic recoil system, which is mostly along the η axis. Good balance along ξ selects events with well measured invariant mass. This “ p_T constrained sample” brings the total UA2 Z sample to 148 events compared to 73 electron pairs and 132 muon pairs at CDF. Backgrounds to these samples are estimated to be less than 1%.

4b. Lepton energy calibration

Certain straightforward elements of the lepton energy calibration strategy are common to both experiments. An “electron cluster” is defined as the merged information from the small number of calorimeter towers (3/2 at CDF/UA2) that contain most of the energy. The calorimeter response to electrons is measured in a test beam:

$$\sigma_{E_T}^{\text{CDF}} = 13.5\% \sqrt{E_T} \quad \sigma_E^{\text{UA2}} = 17\% \sqrt{E}$$

Response maps are derived to correct for variation in the calibration across the face of each tower. Clusters near towers edges and boundaries, where the measurement is unreliable, are rejected. Finally, note that some of the soft hadrons produced in association with the vector boson (the “underlying event”) will occasionally be superimposed with the electron. An average correction for this effect is measured in $W \rightarrow e\nu$ events

$$\Delta E_{\text{ue}}^{\text{CDF}} = -60 \pm 5 \text{ MeV} \quad \Delta E_{\text{ue}}^{\text{UA2}} = -120 \pm 20 \text{ MeV}$$

and reflects, somewhat, the size difference between the CDF and UA2 calorimeter towers.

The most important, and most difficult, issue for the lepton energy calibration is the determination of the absolute energy scale. UA2 relies on the test beam calibration.

All calorimeter towers were measured before installation, and the scale has been tracked using periodic source and pulser measurements. Each year, a part of the calorimeter is recalibrated in the test beam to check this procedure, yielding an estimated error of 1% on the absolute energy scale.

At CDF, the calorimeter scale can be cross calibrated with that of the magnetic tracking system. Systematic misalignments in the tracking system will produce a charge dependent sagitta error:

$$\frac{1}{p_{\pm}} = \frac{1}{p_{\text{true}}} \pm \frac{1}{\Lambda}$$

However, errors in the scale of any calorimetry cell are charge independent

$$E_{\pm}^i = E_{\text{true}} (1 + \epsilon^i)$$

Taking the ratio, and then sums and differences of the above, it is easy to see that, to lowest order in the small corrections $E/p)_+^i + E/p)_-^i$ measures ϵ^i and $E/p)_+ - E/p)_-$ measures Λ .

A large sample of electrons from W decay is used in conjunction with the sum above to provide a measure of the cell-to-cell variations, ϵ^i , in the calorimeter, at the expense of an additional small statistical error:

$$\sigma_{E_T}^{\text{CDF}} = 13.5\% \sqrt{E_T} \oplus 1.7\%$$

The same sample is used in conjunction with the difference above to derive corrections to the tracking geometry that minimize Λ . The scale error in the ‘‘corrected’’ tracking system is measured by comparison of J/ψ and Υ masses with the world averages, and found to be small in relation to the error in the comparison, 0.2%, which is taken to be the tracking scale uncertainty.

Finally, the calorimeter scale can be tied to the precisely known tracking scale by the requirement that the global E/p distribution in the $W \rightarrow e\nu$ sample be consistent with that predicted by a radiatively corrected Monte Carlo analysis. The final error on the calorimeter scale at CDF is estimated to be 0.4%.

Regards the CDF muon sample, the measured muon momentum has the CTC accuracy described in Sec. 3, $\delta p_T/p_T^2 \cong 0.1\% (\text{GeV}/c)^{-1}$, and the muon scale error is just the 0.2% track scale error discussed above.

4c. The M_Z fit and results

Both experiments fit the $\ell^+\ell^-$ invariant mass distribution to a quasi-analytic line-shape representing the convolution of a Breit-Wigner decay with parton structure functions and a Gaussian resolution function which is applied event by event with the measured error. The Z width is fixed at 2.5 GeV. The electron measurements utilize calorimetry and the CDF muon measurement utilizes the charged tracking system. After a small (0.1%) correction for radiative effects of the kind $Z \rightarrow e^+e^-\gamma$, the Z mass is measured to be

			<u>Stat</u>		<u>Sys</u>		<u>Scale</u>			
CDF:	$M_Z^{e^+e^-}$	=	91.1	\pm	0.3	\pm	0.4	\pm	0.2	GeV/c ²
CDF:	$M_Z^{\mu^+\mu^-}$	=	90.7	\pm	0.4	\pm	0.1	\pm	0.2	GeV/c ²
UA2:	$M_Z^{e^+e^-}$	=	91.49	\pm	0.35	\pm	0.12	\pm	0.92	GeV/c ²

where the statistical, systematic, and scale uncertainties are listed separately.

All the measurements have similar statistical precision. The large systematic uncertainty on the CDF electron result arises mostly in the calorimeter/tracking calibration match, and might be considered another component of the scale uncertainty. The UA2 measurement relies on calorimetry alone, and is completely dominated by the scale error.

Combining statistical and systematic uncertainties, and combining the two CDF results into a weighted average, the results of the Z mass measurement are

CDF:	M_Z	=	90.9	\pm	0.3	\pm	0.2	GeV/c ²
UA2:	M_Z	=	91.49	\pm	0.37	\pm	0.92	GeV/c ²

These results are consistent with the results from LEP/SLC, but obviously inferior in precision. As demonstrated below, however, they have great utility when used in concert with other measurements. More detail on the CDF and UA2 Z mass results can be found in Refs. 2 and 4.

5. The Measurement of M_W

W decays in both experiments are detected and isolated in the leptonic decay mode

$$W \rightarrow \ell\nu_\ell$$

The treatment of charged lepton energy is identical to that in the M_Z analysis. The neutrino kinematics are reconstructed from the transverse energy imbalance measured in the “missing E_T ”

$$E_T^\nu = \vec{E}_T = - \sum_i E_{T_i} \cdot \hat{n}_i$$

where the sum extends over all calorimeter cells. The best measurement of the W mass is derived from a fit to the lineshape of the “transverse mass”

$$M_T^2 = 2E_T^e E_T^\nu (1 - \cos \Delta\phi_{e\nu})$$

where $\Delta\phi_{e\nu}$ is the angle between the electron and the neutrino. The systematics of the measurement depend crucially on understanding the measurement of missing E_T in each detector.

5a. Event selection

The triggers for $W \rightarrow \ell\nu_\ell$ events utilize the charged final state leptons, and are identical to the Z decay case, as is the offline treatment of the lepton. Further selection criteria are summarized in Table 2. The missing E_T measurement is most reliable when uncomplicated by the motion of the W . A sample of W 's approximately at rest is culled by explicit cuts on the E_T^W , or by restrictions on other jet activity in the event. At CDF, additional cuts are used to reject dijet background and events with poorly measured \cancel{E}_T . W decays are required to have a lepton and a neutrino above an E_T threshold, and a transverse mass in a broad range around the previously measured value. Small backgrounds, mostly from the sequential decay $W \rightarrow \tau\nu \rightarrow \ell\nu\nu$, are estimated from Monte Carlo.

The final CDF sample has 1130 events in the electron channel and 592 in the muon channel. The UA2 sample has 1203 electronic decays.

5b. Neutrino energy calibration

The precision of the neutrino E_T measurement via \vec{E}_T relies critically on understanding the response of the calorimeter to the uncorrelated underlying event, as well as to any low energy hadronic system recoiling against the W . Achieving the most accurate results and understanding the uncertainty of the \vec{E}_T measurement is the most difficult aspect of

the M_W analysis. The outline of the CDF and UA2 analyses again proceed in somewhat similar fashion, as outlined below.

First, it is convenient to separate the calorimeter response into a component coming from the charged lepton, and the more problematic component due to the low energy hadrons. Define, then, the "underlying event" \vec{u} , such that

$$\begin{aligned}\vec{E}_T^{\text{total}} &= \vec{E}_T^\ell + \vec{E}_T^\nu + \vec{u} = 0 \\ \vec{E}_T^\nu &= -\vec{E}_T^\ell - \vec{u} \quad \text{where } \vec{u} = \sum_{\not\ell} E_{T_i} \cdot \hat{n}_i\end{aligned}$$

where $\not\ell$ signifies that the sum is over all calorimeter cells except the 2 or 3 which contain the lepton cluster. The resolution in \vec{u} , σ_u , can be studied in events collected with a "minimum bias" trigger, where we expect to find $\langle |\vec{u}| \rangle = \langle |\vec{E}_T| \rangle = 0$. Since \vec{u} depends on the cumulative effect of many measurements with common variance, its error should scale approximately like $\sqrt{E_T^{\text{total}}}$. This is borne out by measurement, and is parameterized as:

$$\text{CDF : } \sigma_u = 0.56 \sqrt{E_T^{\text{total}}} \quad \text{UA2 : } \sigma_u = 0.8 (E_T^{\text{total}})^{0.4}$$

Next, a response function is derived to correct for the error associated with assuming that $E_T^W = E_T(\text{hadronic recoil})$, when, in fact, the measurement of the recoil E_T is confused by the nonlinearity of the uncompensated calorimeters, and the calorimeter acceptance. UA2 derives a functional form for the response based on Monte Carlo studies. At CDF, the response is derived from a study of the momentum balance along the ξ axis in the large Z sample, and is applied as a momentum dependent, multiplicative rescaling of \vec{u} . At high E_T^W , the response is scaled by a factor of 1.4.

Finally, small corrections are made for unavoidable errors in the separation of the lepton from the underlying event. These are

1. The amount of underlying energy accidentally removed:

$$\text{CDF : } +60 \pm 5 \text{ MeV} \quad \text{UA2 : } +120 \pm 20 \text{ MeV}$$

2. The contribution from electron shower tails outside of the fiducial cluster area which should have been removed, but were not:

$$\text{CDF : } -260 \pm 20 \text{ MeV} \quad \text{UA2 : } -170 \text{ MeV}$$

At CDF, analogous corrections are made for energy deposited by the minimum ionizing muon. Note that the first set of numbers are identical to those discussed in the context of lepton energy measurement in Sec. 4b.

Some checks on the above procedures will be described in Sec. 5d.

5c. The M_W Fit

Since there is no measurement of the longitudinal momentum of the neutrino in the $W \rightarrow \ell\nu$ sample, the W mass measurement must rely on purely transverse quantities. Lepton and neutrino E_T depend directly on the unknown E_T^W distribution. The transverse mass distribution is less sensitive to E_T^W , but depends critically on detector resolution and acceptance. The complexity and uncertainty of the situation make an analytic lineshape impossible for any transverse distribution. The strategy of both experiments thus relies on model lineshapes generated via Monte Carlo.

Simple models for the physics and the detector are used to generate a table of likelihoods for a large number of discrete W masses and widths. These tables are interpolated and smoothed to create likelihood distributions that can be fit to data distributions using the maximum likelihood technique. The consistency of the method is checked by examining the fit results for large Monte Carlo generated event samples with known masses and widths. The effect of small systematic effects can be studied by varying the model parameters, generating new likelihoods, and evaluating the change in fits for the Monte Carlo samples.

The Monte Carlo models are elementary and malleable, using simple parameterizations of the separable effects, and when possible, deriving these parameterizations from the data itself. The elements of the models for both experiments include:

1. W decay: Simple 4-vector generator with Breit-Wigner decay, polarization, and vertex smearing.
2. $f(x)$: CDF uses MRSB, UA2 uses DFLM, with $\Lambda = 160$ MeV. Both experiments test many others.
3. Lepton energy: Parameterized as in the $Z \rightarrow \ell^+\ell^-$ analysis.
4. Underlying event: Generated according to the description in Section 4b.

5. E_T^W : CDF adjusts to fit distribution in data. UA2 uses Altarelli, Ellis, et al.[10], and examines the effect of variation in Λ_{QCD} .
6. Detector: Derived from data, test beam, and Monte Carlo Studies as described in Sections 4b and 5b.

As an example, consider the reconstruction of the neutrino kinematics. Starting with a W with some non-zero E_T as parameterized in (5), the decay in (1) generates a neutrino E_T which is then converted to missing E_T in a manner which incorporates the nonlinear detector response in (6), and includes also the effect of an uncorrelated underlying event generated according to the prescription in (4).

5d. Estimates of systematic uncertainty

The reliability of the detector and physics model is checked against the data in a variety of ways. The parameterization of the recoil response can be examined by the energy balance in the η direction in Z events, which is sensitive to the recoil systematics and not to the lepton energy resolution. The situation at UA2 is shown in Fig. 4. The width of this distribution is sensitive to σ_u , and the mean is sensitive to the accuracy of the E_T^W distribution and the calorimeter response. The model result is shown as the solid curve and is seen to provide a good representation of the data.

The corrections for energy flow into and out of the lepton cluster, discussed at the end of Section 5b, are studied in "parallel balance" at CDF. As seen in Fig. 5, the underlying event can be decomposed into components parallel and perpendicular to the lepton direction, and $\bar{u}_{||}$ is sensitive to errors in the lepton removal. The distribution of this quantity has $\langle u_{||} \rangle = -76 \pm 115$ MeV. The error here is a measure of the accuracy of the scheme; the offset, although less than one standard deviation, is incorporated into the model.

Effects of structure functions, backgrounds, and fitting procedures are also modelled. The results from study of all anticipated effects are listed for both experiments in Table 3. CDF and UA2 differ in the relative weights of the various components, but the end result, surely due to conservation of difficulty, is a systematic error in the range of 200-300 MeV for both experiments.

5e. The M_W result

Finally, the model derived lineshapes for a W with fixed width of 2.1 GeV are fit to the measured M_T distribution using a maximum likelihood technique. The results are shown in Fig. 6, and, after a small (0.1%) correction for radiative effects, yield the following results:

			<u>Stat</u>		<u>Sys</u>		<u>Scale</u>			
CDF:	M_W^e	=	79.81	±	0.33	±	0.25	±	0.34	GeV/c ²
	M_W^μ	=	79.86	±	0.58	±	0.33	±	0.16	GeV/c ²
UA2:	M_W	=	80.79	±	0.31	±	0.21	±	0.81	GeV/c ²

The UA2 measurement is dominated by the scale error. The best precision on the absolute mass scale is achieved by calculating the ratio M_W/M_Z , where the scale error virtually cancels, and then normalizing to the precise Z mass measured at LEP/SLC. At CDF, this is less important, but done anyway, with a least squares technique that keeps track of the error correlations between the electron and muon measurements. The results of this rescaling are

$$\text{CDF: } M_W = 79.92 \pm 0.45 \text{ GeV}/c^2$$

$$\text{UA2: } M_W = 80.49 \pm 0.49 \text{ GeV}/c^2$$

where the two CDF results have been averaged, and all errors have been added in quadrature. The results of the two experiments are consistent. More detail on the CDF and UA2 W mass results can be found in Refs. 3 and 4.

6. The Standard Model Parameters

The interrelation between the parameters M_Z , M_W , M_{top} , and M_H can now be examined in a number of interesting ways. Fig. 7 is based on the work of Hollik and Burgers[8][4], and shows the contours of constant M_{top} in the $M_W - M_Z$ plane. Assuming that the CDF and UA2 W results are completely independent, their weighted mean gives the best "World Average" W mass to date as

$$M_W = 80.18 \pm 0.33 \text{ GeV}/c^2$$

I have superposed this result on Fig. 7, along with the current best M_Z from the weighted average of LEP results:[11]

$$M_Z = 91.161 \pm 0.031$$

It is clear that the measurements are honing in on M_{top} . Note that without radiative corrections the vector boson masses are $M_W^0 = 77.7 \text{ GeV}/c^2$ and $M_Z^0 = 89.0 \text{ GeV}/c^2$, and thus not even on this plot. The precision of the current measurements is, indeed, much smaller than the scale of the radiative corrections, and tests the perturbative expansion of the theory.

The correlation of M_W and M_{top} is displayed more directly in Fig. 8, where Barger, Hewett, and Rizzo[12] add even yet higher order corrections to the program of Morris, which is based on the work of Hollik. The Z mass is taken to be $91.172 \text{ GeV}/c^2$. The central value and the 90% confidence band limit for the CDF/UA2 mass value is superimposed, and leads to a limit

$$80 \text{ GeV}/c^2 < M_{\text{top}} < 230 \text{ GeV}/c^2 \quad (90\% \text{CL})$$

on the mass of the top quark. This result is consistent with the implications of Fig. 7. and with the result of direct searches. Note that approximately 30 GeV at each end of the interval above can be attributed to the uncertainty in the Higgs mass.

Finally, contact with earlier results can be made by using the standard Marciano-Sirlin definition, Eq. 1, to unambiguously derive $\sin^2 \theta_W$ from the ratio of the vector boson masses. This derivation includes the experimental bonus of cancellation of the mass scale error in the two measurements and is another good reason for measuring M_Z at the hadron collider experiments. The results are

$$\text{CDF: } \sin^2 \theta_W = 0.231 \pm 0.008$$

$$\text{UA2: } \sin^2 \theta_W = 0.220 \pm 0.010$$

Combining in a weighted average, the best "World Average" from hadronic colliders to date is then

$$\sin^2 \theta_W = 0.227 \pm 0.006$$

This can be compared to a global fit to all deep-inelastic data by Amaldi et al.[13].

$$\sin^2 \theta_W = 0.233 \pm 0.005$$

assuming $M_{\text{top}} = 45 \text{ GeV}/c^2$, and $M_H = 100 \text{ GeV}/c^2$. The collider result is competitive in precision, and independent of any assumptions about M_{top} and M_H .

7. The Forward-Backward Asymmetry in $Z \rightarrow e^+e^-$.

A completely independent measure of $\sin^2 \theta_W$ is available in the charge asymmetry of the decay angular distribution in $Z \rightarrow e^+e^-$. The lowest order cross section for this decay is the sum of photon and Z contributions plus an interference term:

$$\begin{aligned} \frac{d\sigma^\gamma}{d\Omega} &\propto (1 + \cos^2 \hat{\theta}) \\ \frac{d\sigma^I}{d\Omega} &\propto g_V^e g_V^q (1 + \cos^2 \hat{\theta}) + 2g_A^e g_A^q \cos \hat{\theta} \\ \frac{d\sigma^Z}{d\Omega} &\propto (g_V^e{}^2 + g_A^e{}^2)(g_V^q{}^2 + g_A^q{}^2)(1 + \cos^2 \hat{\theta}) + 8g_V^e g_A^e g_V^q g_A^q \cos \hat{\theta} \end{aligned}$$

where the vector and axial vector couplings are

$$g_A^f = T_3^f \quad g_V^f = T_3^f - 2Q_f \sin^2 \theta_W$$

and $\hat{\theta}$ is the angle between the outgoing electron and the incoming quark. The quasi-left-handedness of the couplings produces the infamous $\cos \hat{\theta}$ term which describes the charge asymmetry. On the Z pole, the interference term is small, the Z term is large, and the asymmetry measures $\sin^2 \theta_W$. This measurement is distinguished from its LEP counterpart by its sensitivity to the quark vector couplings and thus greater magnitude since, at LEP, the coefficient of the $\cos \hat{\theta}$ term contains *two* powers of the small electron vector coupling.

CDF has measured the charge angular asymmetry in a sample of events selected in a manner very similar to that of the Z mass sample. $\hat{\theta}$ is the angle between the proton and the final state electron in the Z rest frame. The assumption that the quark is in the proton will be wrong half the time in the 15% of interactions which are sea-sea, leading to a small symmetric background. Transverse motion of the quark is handled with the Collins-Soper[14] formalism. Complications from detector acceptance are small, since the charge independence of electron detection implies that the acceptance must be symmetric in $\cos \hat{\theta}$. Fig.9 shows a maximum likelihood fit of the full cross section, including interference term, to 250 events with $75 \text{ GeV}/c^2 \leq M_{e^+e^-} \leq 105 \text{ GeV}/c^2$. The front-back asymmetry is defined as usual

$$A_{fb} = \left(\int_{c=0}^{c=1} d\sigma - \int_{c=-1}^{c=0} d\sigma \right) / \int_{c=-1}^{c=1} d\sigma \quad \text{where } c = \cos \hat{\theta}$$

The results of the analysis are summarized in Table 4. $\sin^2 \theta_W$ is derived from the likelihood fit, and is meaningful only to lowest order. The corrections for background and

non-zero quark E_T are small, as well as that due higher order QED corrections. Unlike the calibration dominated mass measurements, the systematic errors here are all very small, and the precision is completely dominated by the statistical error.

As expounded in Sec. 2, comparison of this $\sin^2 \theta_W$ to other measurements requires accounting for the higher order weak effects particular to this process and conversion to the Marciano-Sirlin standard. An iterative solution for the value of $\sin^2 \theta_W$ which generates the observed asymmetry is shown, as a function of M_{top} in Fig 10. M_H is taken as $100 \text{ GeV}/c^2$. Superimposed is the value of $\sin^2 \theta_W$ derived from the CDF vector boson mass ratio. The dotted lines indicate the band of 1σ in precision. The two completely independent measurements are consistent over the entire allowed range of M_{top} .

8. Conclusion

Careful attention to energy calibration, along with data driven understanding of systematic effects, allow CDF and UA2 to measure the mass of the W boson with unprecedented accuracy:

$$\text{CDF: } M_W = 79.92 \pm 0.45 \text{ GeV}/c^2$$

$$\text{UA2: } M_W = 80.49 \pm 0.49 \text{ GeV}/c^2$$

Derived results from these measurements include:

$$\sin^2 \theta_W = 0.227 \pm 0.006$$

$$80 \text{ GeV}/c^2 < M_{\text{top}} < 230 \text{ GeV}/c^2 \quad (90\% \text{CL})$$

An alternative measurement of $\sin^2 \theta_W$ from the front-back asymmetry in $Z \rightarrow e^+e^-$, at CDF, has systematic error of a mere 0.002, and is only statistics limited. Larger data sets and increased understanding of the detectors promise a future of precise results which test the consistency of the Standard Model.

I acknowledge the hard work of my CDF collaborators, and helpful discussions with P. Hurst, L. DiLella, and M. Golden.

References

- [1] B. Adeva et al., Phys. Lett. B(231), 509 (1989), D. Decamp et al., Phys. Lett. B(231), 519 (1989), M. Akrawy et al., Phys. Lett. B(231), 530 (1989), P. Aarnio et al., Phys. Lett. B(231), 539 (1989).
- [2] F.Abe et al., Phys. Rev. Lett., 63, 720 (1989).
- [3] F.Abe et al., to be published in Phys. Rev. Lett. and in Phys. Rev. D.
H. Jensen, CDF Collaboration, talk given at the Meeting of the American Physical Society, Washington DC, April 16-19 1990.
- [4] J. Alitti et al., CERN-EP/90-22 preprint (1990). To be published in Physics Letters B.
- [5] L.DiLella, CERN-EP/88-02 preprint (1988).
- [6] W.J.Marciano, A.Sirlin, Phys. Rev. D22, 2695 (1980).
- [7] See, e.g. discussion in Ref. 12, and references therein.
- [8] W.Hollik, G.Burgers, Z Physics at LEP1, Vol. 1, CERN 89-90.
- [9] F.Abe et al., Nucl. Instrum. Methods Phys. Res., Sect. A271, 387 (1988).
- [10] G.Altarelli, R.K.Ellis, M.Greco, G.Martinelli, Nucl. Phys. B246, 12 (1984).
- [11] The Particle Data Group, Phys. Lett. 1990. To be published.
- [12] V.Barger, J.L.Hewett, T.G.Rizzo, University of Wisconsin preprint MAD/PH/564 (1990).
- [13] U. Amaldi et al., Phys. Rev. D36, 1385 (1987).
- [14] J. C. Collins and D. E. Soper, Phys. Rev. D16, 2219 (1977).

Table 1. Z sample selection

Selection	CDF	UA2
a. Triggers		
single e:	$E_T^{em} \geq 12 \text{ GeV}$ $P_T^{trk} \geq 6 \text{ GeV}/c$	$E_T^{em} \geq 12 \text{ GeV}$
double e:	$2E_T^{em} \geq 10 \text{ GeV}$	$2E_T^{em} \geq 6 \text{ GeV}$
single μ :	Stub in CMU $P_T^{trk} \geq 9 \text{ GeV}/c$	
double μ :	2 stubs in CMU $2P_T^{trk} \geq 3 \text{ GeV}/c$	
b. Lepton ID		
electron:	track/shower match lateral shower profile longitudinal shower profile $E/p \leq 1.4$	
muon:	track/stub match $E_{em} \leq 2 \text{ GeV}$ $E_{had} \leq 6 \text{ GeV}$	
c. Kinematics	$50 \leq M_{ll} \leq 150 \text{ GeV}$	$70 < M_{e^+e^-} < 120 \text{ GeV}$
d. Backgrounds	$\lesssim 1\%$	$\lesssim 1\%$
e. Final sample		
electron:	73 central/central	54 central/central 94 central/elsewhere (P_T constrained)
muon:	132 central/central	

Table 2. W sample selection

Selection	CDF	UA2
a. Triggers	same as $Z \rightarrow l^+ l^-$	
b. Lepton ID	same as $Z \rightarrow l^+ l^-$	
c. \cancel{E}_T quality (neutrino ID)	no jet $E_T \geq 7$ GeV $ \cancel{E}_T \gtrsim 4\sigma_{\cancel{E}_T}$ no jet $E_T \geq 5$ GeV opposite lepton	$E_T^W \leq 20$ GeV
d. Kinematics	$E_T^l \geq 25$ GeV $E_T^\nu \geq 25$ GeV $50 \leq M_T \leq 100$ GeV remove cosmics, Zs	$20 \leq E_T^l \leq 60$ GeV $20 \leq E_T^\nu \leq 60$ GeV $40 \leq M_T \leq 120$ GeV
e. Backgrounds	$\lesssim 1\%$	$\lesssim 3\%$
f. Final sample	1130 $W \rightarrow e\nu$ 592 $W \rightarrow \mu\nu$	1203 $W \rightarrow e\nu$

Table 3a M_W systematics summary for CDF

	Electrons	Muons	Common
SYSTEMATICS	240	315	150
1. Proton structure	60	60	60
2. Resolution, W_{PT}	145	150	130
3. Parallel balance	170	240	
4. Background	50	110	
5. Fitting	50	50	50

Table 3b M_W systematics summary for UA2

Model Variation	m_T Fit
1. Hadron Resolution/ Response and P_T (boson) Distribution	± 115
2. Parton Distributions	± 100
3. Neutrino Scale	± 85
4. Electron Resolution	± 40
5. Underlying Event	± 30
6. Fit Procedure	± 100
7. Radiative Decays	$+40 \pm 40$
Total	$+40 \pm 210$

Table 4: Summary of results for the Z asymmetry analysis.

From the log likelihood fits the following values are obtained:

$$\begin{aligned} A_{FB} &= 0.0500 \pm 0.0587 \text{ (stat)} \\ \sin^2 \theta_W &= 0.2314 \pm 0.0158 \text{ (stat)} \end{aligned}$$

The following corrections are made to A_{FB} and $\sin^2 \theta_W$:

	ΔA_{FB}	$\Delta \sin^2 \theta_W$
Background subtraction	0.0014	-0.0004
QCD (PT) corrections	0.0008	-0.0002
QED corrections	0.0055	-0.0014

The systematic uncertainties are measured to be:

	σA_{FB}	$\sigma \sin^2 \theta_W$
Background subtraction	0.0006	0.0002
$\ln \mathcal{L}$ fitter	0.0026	0.0008
Electron trigger	0.0018	0.0005
Track reconstruction	0.0002	0.00005
Electron selection	0.0001	0.00003
Structure functions		0.0004
QED corrections	0.0054	0.0016

After adding the systematic uncertainties in quadrature and applying corrections, the results are

A_{FB}	$=$	0.058	\pm	0.059 (stat)	\pm	0.006 (sys)
$\sin^2 \theta_W$	$=$	0.229	\pm	0.016 (stat)	\pm	0.002 (sys)

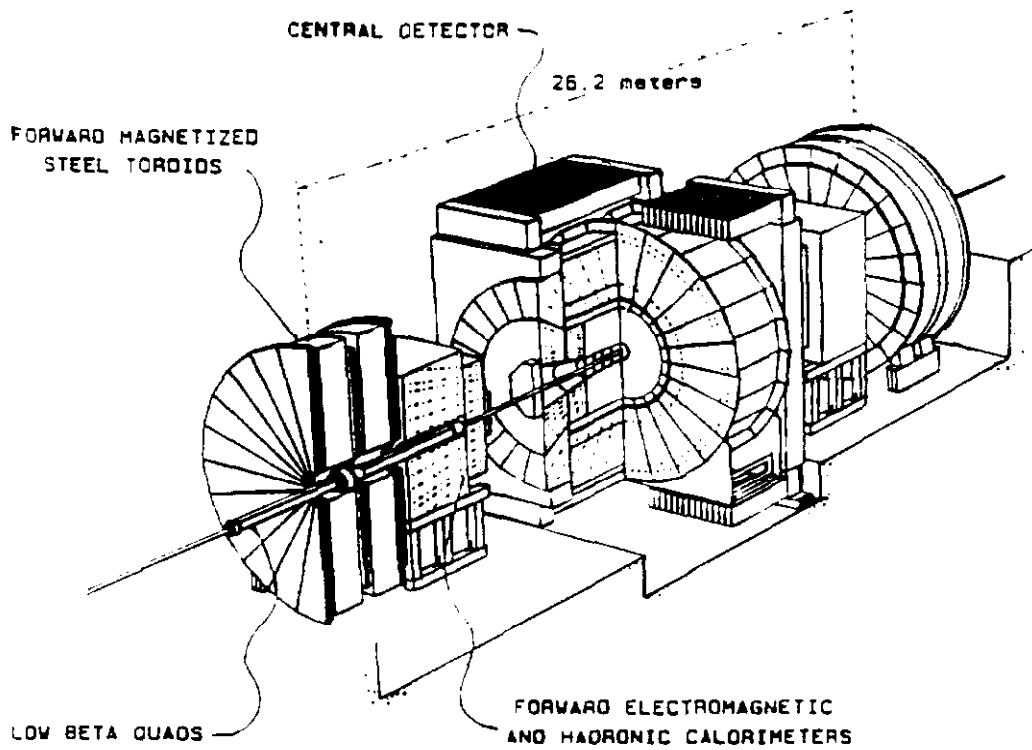


Fig. 1. The CDF Detector

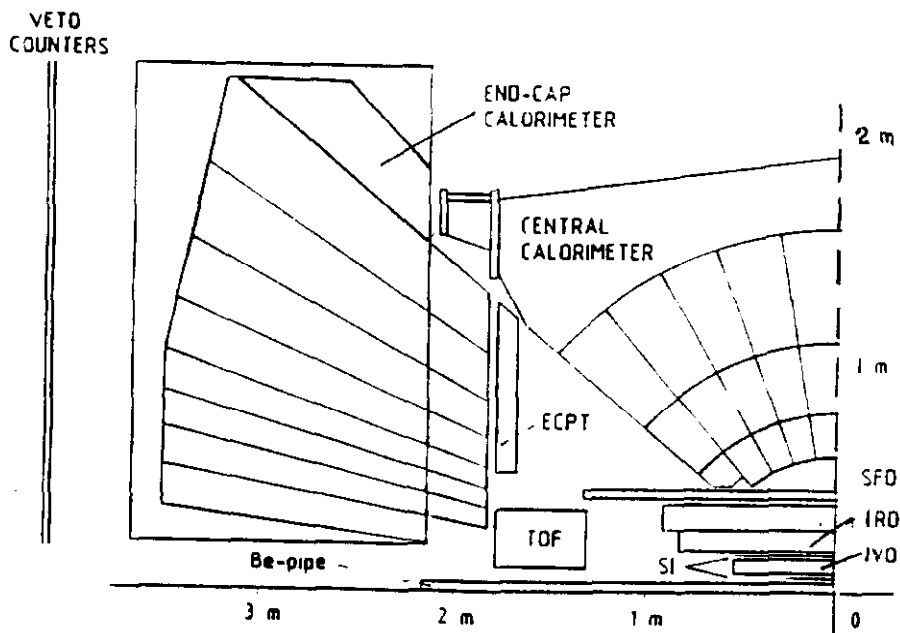


Fig. 2. Cross Section of the UA2 Detector.

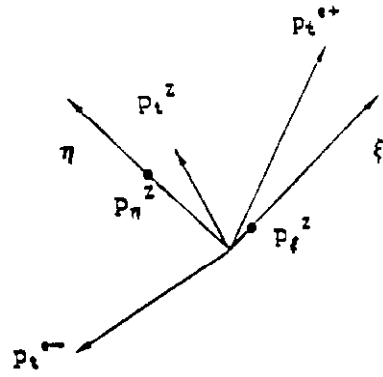


Fig. 3. The $\xi - \eta$ decomposition in $Z \rightarrow e^+e^-$ events.

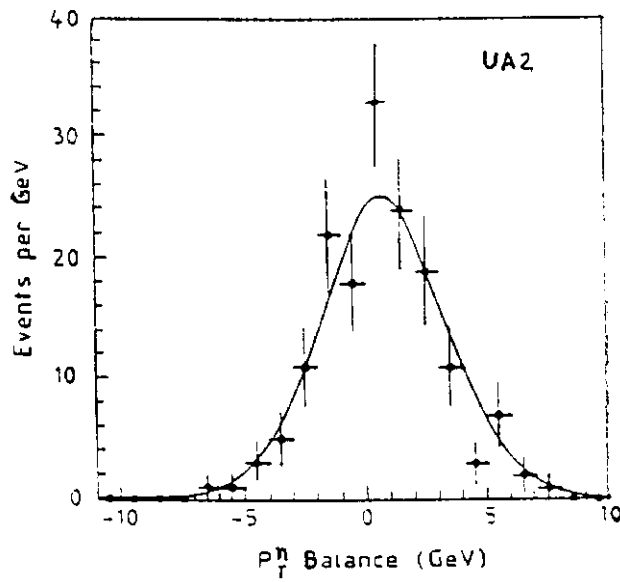


Fig. 4. The recoil momentum balance in $Z \rightarrow e^+e^-$ events in UA2.

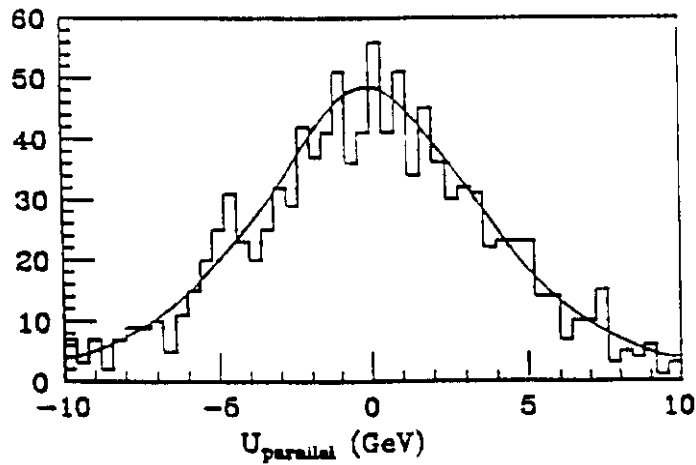


Fig. 5. The parallel balance in $W \rightarrow e\nu$ events in CDF.

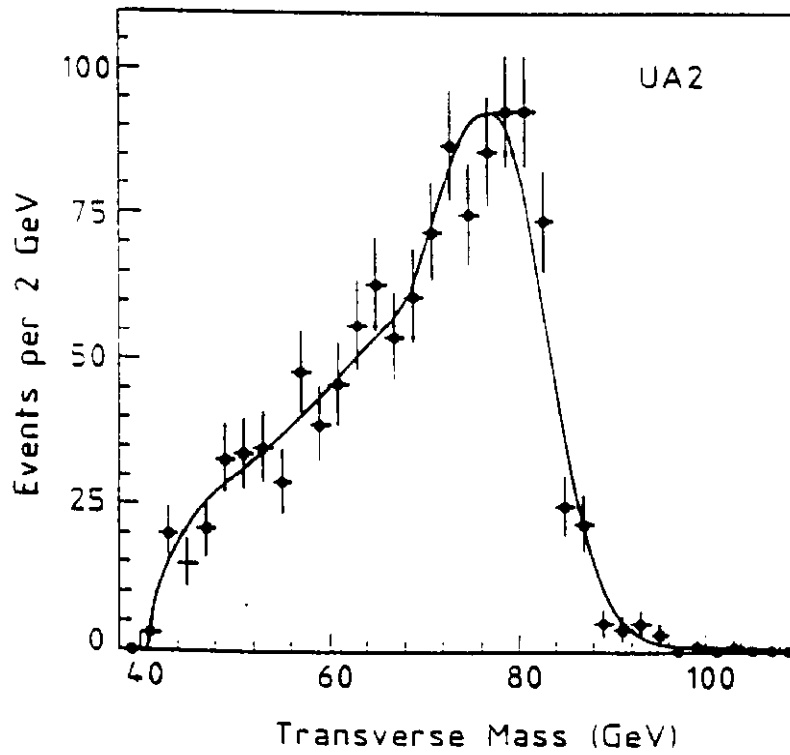
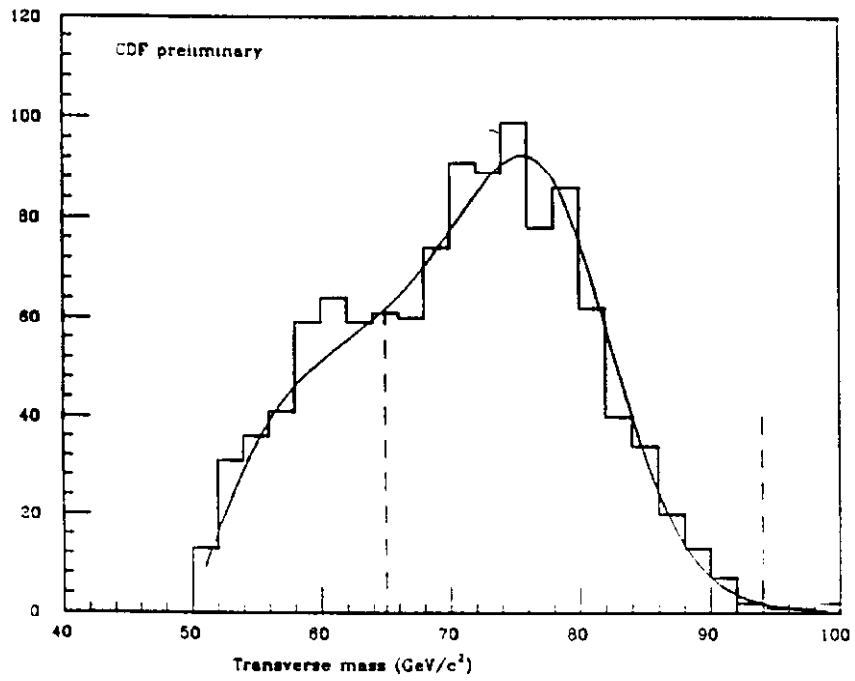


Fig. 6. The transverse mass distribution for $W \rightarrow e\nu$ events in CDF (top) and UA2 (bottom).

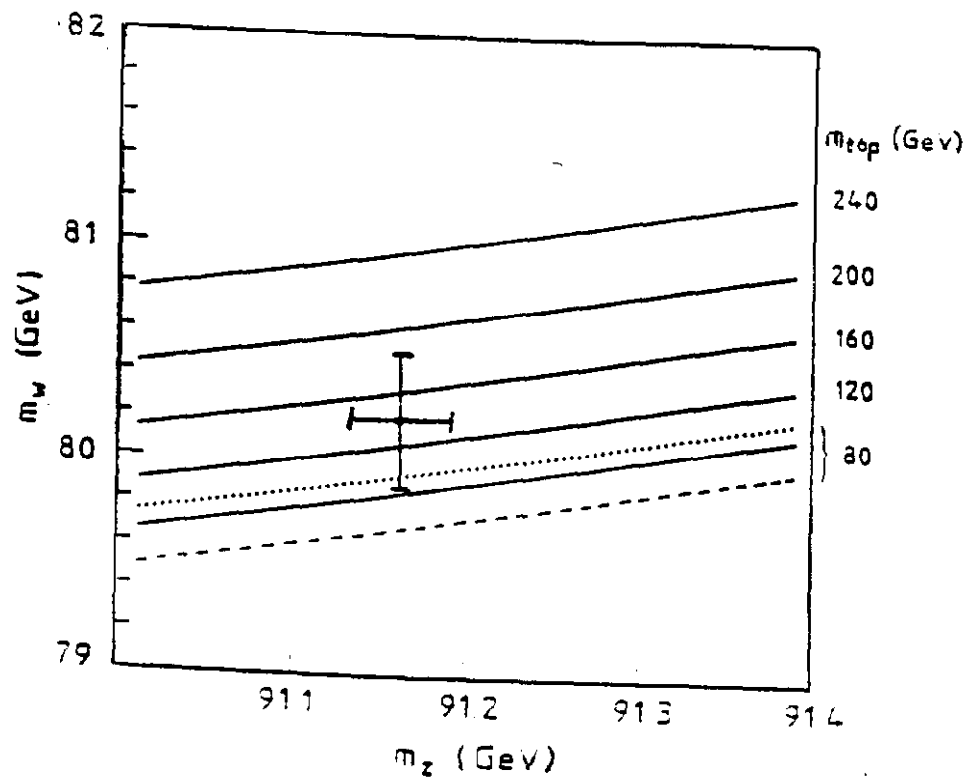


Fig. 7. Contours of constant M_{top} in the $M_W - M_Z$ plane, and current weighted mean values for the vector boson masses, with 1σ errors.

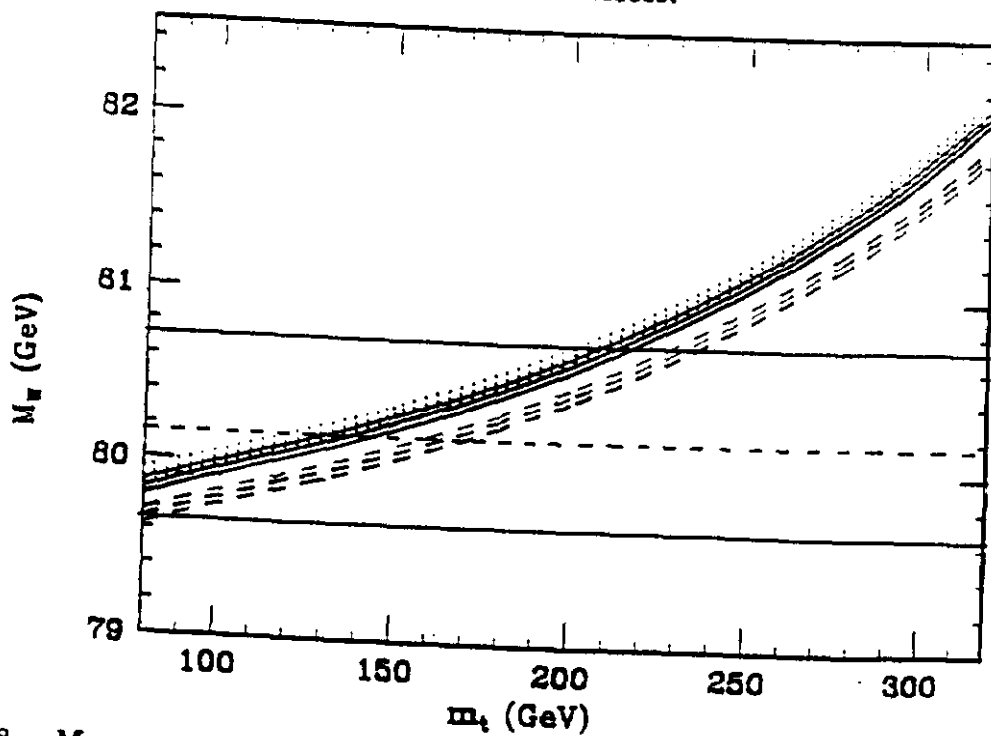


Fig. 8. M_W versus M_{top} , and the 90% confidence interval on the CDF/UA2 M_W determination.

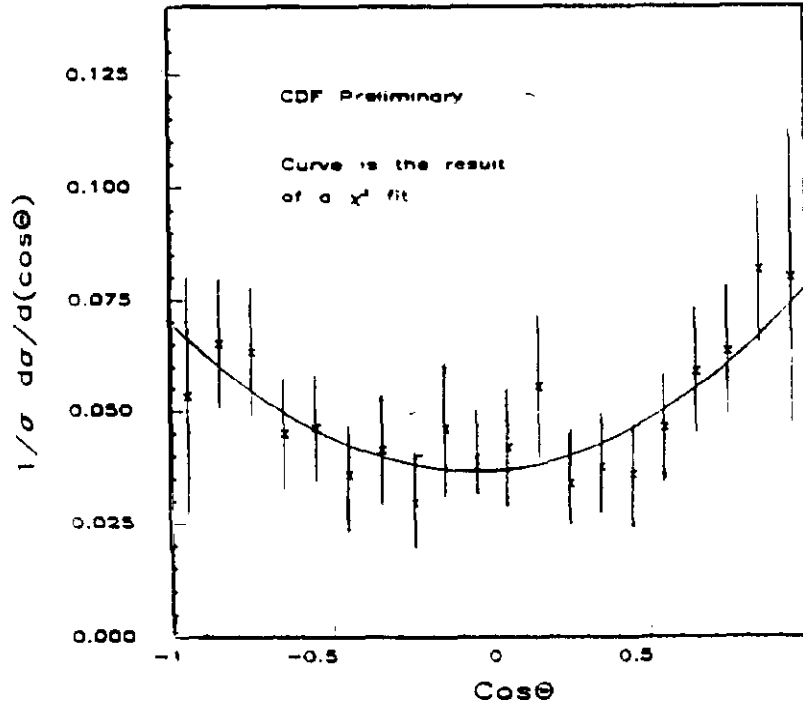


Fig. 9. The $\cos \hat{\theta}$ distribution in $Z \rightarrow e^+e^-$ at CDF, and fit to lowest order cross section.

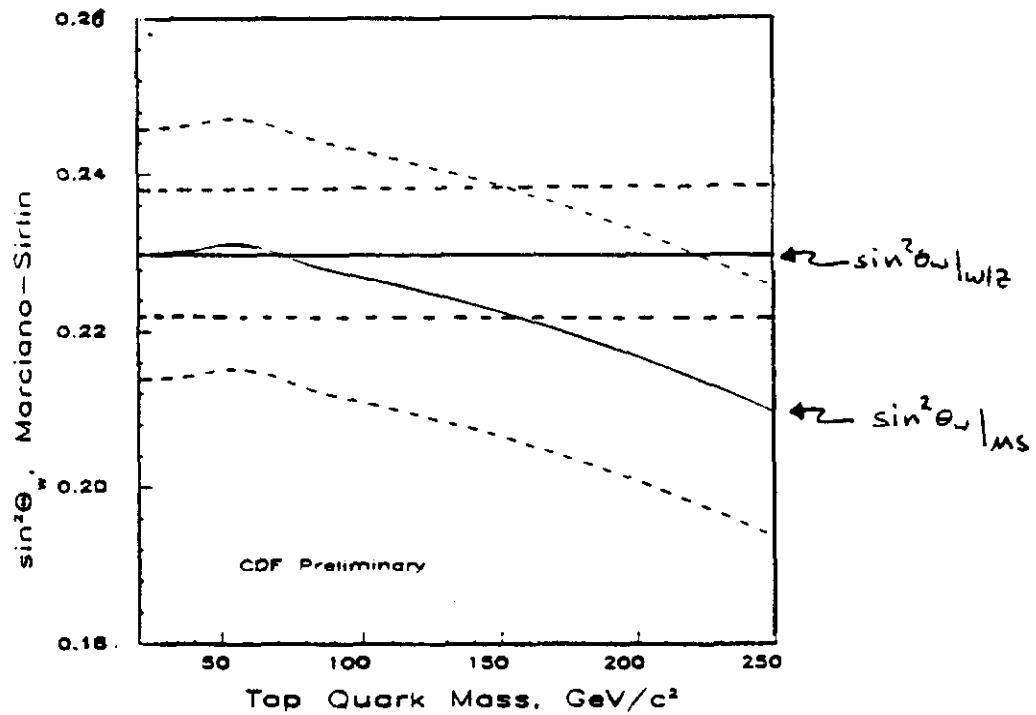


Fig. 10. The Marciano-Sirlin value for $\sin^2 \theta_W$ which produces the observed asymmetry in $Z \rightarrow e^+e^-$, as a function of M_{top} . Superposed is the value of $\sin^2 \theta_W$ from the M_W, M_Z measurement.